Int. J. Heat Mass Transfer. Vol. 36, No. 7, pp. 1739–1748, 1993
Printed in Great Britain

0017-9310/93 $6.00+0.00

Turbulence model of fire-induced air flow in a ventilated tunnel

H. XUE,† E. HIHARA and T. SAITO
Department of Mechanical Engineering, The University of Tokyo, 7-3-1 Hongo, Bunkyo-ku, Tokyo 113, Japan

(*Received* 20 *February* 1992 *and in final form* 26 *October* 1992)

Abstract—The fire-induced air flow in a ventilated tunnel with a local gas burner is investigated experimentally and numerically. To simulate the transient three-dimensional turbulent buoyancy flow, calculations employ the turbulence k–ε model which is modified to take account of the effects of the mean streamline curvature (MSC). General curvilinear coordinates are generated for the computation. The prediction is compared with the experimental data and shown to be in reasonable agreement except the region close to the heat source. The present model can also be used to predict the location of the leading edge of the heated air flow.

1. INTRODUCTION

THE HEATED air, smoke and toxic gases that are created by a fire within a building, corridor, tunnel or other structure can cause a definite hazard to people. A good physical insight into fire dynamics is desirable for systematic planning of fire safety in design and maintenance. For the case of tunnel fires, a quantitative knowledge about the detailed behavior of the heated air flow in a ventilated tunnel is required for fire detection, control, or extinguish. Therefore, theoretical and experimental approaches of modeling the heated air flow present a challenge for researchers and engineers. Not only are the underlying physical processes difficult to model, but variables such as location of the fire source, geometric space, and ventilation air flow all affect the overall behavior of the heated air flow.

In the last two decades, extensive studies have been conducted on the tunnel fire problems. The scientific approaches can be usually classified into three classes: empirical or experimental modeling, zone modeling and field modeling. The experimental modeling includes the works of Quintiere *et al.* [1], Emori and Saito [2]. This approach is useful in situations where detailed knowledge is not required but an understanding of the physics of the phenomenon is considered sufficient. The limitation of this approach is due to inability to preserve all the significant dimensionless group, because full-scale experiments with statistical significance require a huge amount of cost. For this reason, numerical approaches have been rapidly developed. De Ris [3] created a mathematical model for a fire duct to calculate the convection and diffusion of a fire flame and the heated air flow. Hwang *et al.* [4, 5] presented a two-dimensional model to describe the phenomenon of reversed stratified flow in a fire duct. These so-called zone models are based on certain kinds of similarities to calculate the fire plume or the heated air flow in several areas. They have to simplify considerably the complex physical phenomena to keep computational requirements within reasonable bounds and rely heavily on empirical data. Because of this defect, a recent development concentrated more on the application of field models, in which general flow equations expressing the balance of heat, mass and momentum are solved. Recent work includes those of Brandeis and Bergmann [6], Koto and Yamanaka [7]. In our previous study [8], a turbulence k–ε model was applied for a two-dimensional flow to predict the behavior of the heated air flow in a ventilated tunnel. The k–ε model constant C_3 was revised to be an empirical function of ventilation Reynolds number and densimetric Froude number. The revision improved the k–ε model's ability of prediction. The field model approach, however, has not yet reached the stage of describing complete air flow in a tunnel fire. The hot plume induced by a local fire, its interaction with the ventilated air flow, and the secondary flow in cross-sections have significant influences on turbulence. These effects have to be taken into account in the turbulence model. Furthermore, the complicated geometry of a tunnel has to be well treated and the computational costs should be cut down.

The present study deals with the heated air flow in a ventilated tunnel. The numerical calculation uses a field approach and employs a turbulence k–ε model which is modified to take account of the effects of mean streamline curvature. General curvilinear coordinates are adopted. An ordinary grid system is employed for the computation and a specific scheme

† Present address: Research Scientist, Department of Civil Engineering, National University of Singapore, 10 Kent Ridge Crescent, Singapore 0511.

NOMENCLATURE

a	coefficient in the discretization equation
b	constant term in the discretization equation
C_1, C_2, C_3	turbulent model constants
C_μ	turbulent model constant
D_H	hydraulic diameter
g	acceleration of gravity
G_B	buoyancy production term in the k and ε equations
G_k	shear production term in the k and ε equations
Gr^*	modified Grashof number, $g\beta qH^4/\nu^2\lambda$
H	height of the tunnel
h	specific enthalpy
k	turbulent kinetic energy
L	turbulence length scale
p	mean pressure
Pr	Prandtl number
q	heat flux of heat source
r, s	spatial coordinates in cylindrical system
R	radius of the experiment tunnel
Re_D	Reynolds number, $D_H u_0/\nu$
R_f	flux Richardson number
S_h	area of heating
T	mean temperature
t	time
U	a contravariant velocity component in ξ direction
u	mean velocity component in x direction
u'	fluctuating velocity component in x direction
V	a contravariant velocity component in η direction
v	mean velocity component in y direction
v'	fluctuating velocity component in y direction
v_h	blowing velocity of gas mixture
W	a contravariant velocity component in ζ direction
w	mean velocity component in z direction
x, y	spatial coordinates in Cartesian system
x_F	position of the leading edge of the heated air flow
z	spatial coordinates in Cartesian and cylindrical system.

Greek symbols

β	thermal expansion coefficient
Γ	exchange coefficient
γ, θ	angular coordinates in cylindrical system
ε	turbulence energy dissipation
λ	thermal conductivity
μ	dynamic viscosity coefficient
μ_t	turbulent viscosity
ν	kinematic viscosity
ξ, η, ζ	spatial coordinates in general curvilinear system
ρ	air density
σ_t	turbulent Prandtl number
Φ	general dependent variable
ϕ	general scalar quantity
ϕ'	fluctuating scalar quantity.

Subscripts

avg	mean value in a cross-section of tunnel
E, P	east and central grid point under consideration
e, w	east and west control-volume face
n, s	north and south control-volume face
t, b	top and bottom control-volume face
0	initial value.

is used to suppress pressure oscillations. The numerical results have been validated by comparing the predictions with the data obtained from the experiments.

2. EXPERIMENTAL WORK

The basic configuration of experimental apparatus is shown schematically in Fig. 1. It mainly consists of a wind tunnel, a heat source, and a measurement system. The tunnel is made of 0.8 mm-thick galvanized iron sheet. The overall length of this facility is 11.8 m, which includes an 8.45 m long test section. The cross-section of the tunnel takes a shape common to a railway and highway tunnel, a horizontal cylinder of 0.25 m in radius with the flat bottom cut out. A sirocco fan is located to offer ventilation into the tunnel at an adjustable flow speed. Before entering the test section, the air flows through a rectifying duct, which is composed of a cylinder of 0.35 m radius and a contraction duct. A screen and a honeycomb are placed inside the cylinder in order to obtain a uniform air flow. A burner consuming city gas is located 1.9 m from the inlet of the test section and laid on the floor. The burner is made of four independent units. Each of the unit includes 72 small nozzles uniformly distributed in 4 rows, from which the air–gas mixture blows out. Each unit is connected to a gas meter such that heat flux of combustion can be calculated from the gas flux measurement. The fresh air used for combustion is offered from an inlet pipe. The mean velocity of the air in the inlet pipe is measured by a hot-wire anemometer to estimate the blowing velocity of the premixed gas mixture.

It is known [9] that the main emission in a clear premixed flame is in the infra-red region, and the radiation in the visible and ultra-violet regions

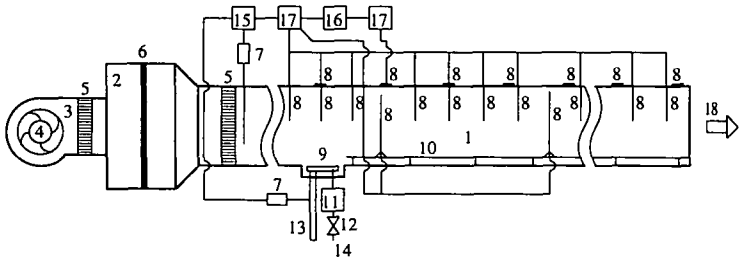

1.Test Section	7.Hot-wire Probe	13.Air Inlet Pipe
2.Settling Chamber	8.Thermocouples	14.Gas Supply
3.Entrance Section	9.Gas Burner	15.Anemometer
4.Sirocco Fan	10.Rail	16.Personal Computer
5.Honeycomb	11.Gas Meters	17.A/D Converter
6.Screen	12 Gas Valves	18. Air Flow

FIG. 1. Schematic of the experiment tunnel.

accounts usually for less than 0.4% of the heat of combustion. For good aeration, only about 10% of the heat of combustion is estimated to be lost in radiation. In the present experiment, the flame is blue–green in color because of premixed combustion. The influence of the radiation is therefore ignored.

To measure the transient temperature distribution in a cross-section and the position of the leading edge of heated air flow, 32 thermocouples are located inside the tunnel. Another 30 thermocouples are placed on the wall surface of the test section to detect the wall temperature which is used as the wall temperature boundary condition in the numerical simulation. The mean velocity of the ventilated air at the tunnel inlet is also measured by a hot-wire anemometer.

3. NUMERICAL ANALYSES

Numerical analyses are carried out under the same conditions as the experiments. The physical problem concerns a three-dimensional tunnel with longitudinal ventilated air flow and with a burner located on the floor, as shown in Fig. 2. As we are mainly interested in the behavior of the heated air flow, the combustion at the burner is simplified as a source with a constant and uniform mass and heat input and is given as boundary conditions in the numerical model.

3.1. *Governing equations*

The turbulent flow is governed by the equations expressing the conservation of mass, momentum, and energy. The Boussinesq approximation is not assumed because the model has to accurately describe flows in which large density variations occur. The equations are written in a Cartesian tensor form

$$\frac{\partial \rho}{\partial t} + \frac{\partial(\rho u_i)}{\partial x_i} = 0, \tag{1}$$

$$\frac{\partial(\rho u_i)}{\partial t} + \frac{\partial(\rho u_i u_j)}{\partial x_j} = -\frac{\partial P}{\partial x_i} + \frac{\partial}{\partial x_j}\left(\mu \frac{\partial u_i}{\partial x_j} - \rho \overline{u_i' u_j'}\right) + g_i(\rho - \rho_0), \tag{2}$$

$$\frac{\partial(\rho \phi)}{\partial t} + \frac{\partial(\rho u_j \phi)}{\partial x_j} = \frac{\partial}{\partial x_i}\left(\Gamma \frac{\partial \phi}{\partial x_i} - \rho \overline{u_i' \phi'}\right) + S_\phi \tag{3}$$

where ϕ represents h, k, or ε. The term S_ϕ means an appropriate source or sink of the variable ϕ concerned.

The present model does not include a conservation equation for some species concentration. By assuming that $\rho' u_i' \ll \rho u_i$, the fluctuation of the density is ignored. Therefore the density is only related to the temperature of the air through the equation of state

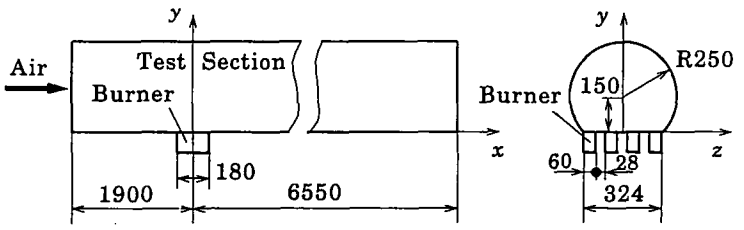

FIG. 2. Sketch of the model tunnel.

$$\rho = \rho(T). \quad (4)$$

The physical properties of air such as thermal expansion coefficient β, viscosity coefficient μ, etc. are given by the polynomial functions of temperature.

3.2. *Turbulence model*

For the closure of the governing equations, the two-equation k–ε model [10] of turbulence is used. In the k–ε model, the knowledge of the local values of k and ε allows the evaluation of a local turbulent viscosity μ_t, that is

$$\mu_t = \rho C_\mu \frac{k^2}{\varepsilon}. \quad (5)$$

Since buoyancy plays an important role in both promoting (in the rising plume) and suppressing (in the ceiling layer) turbulent mixing, an extension to the model suggested by Rodi [11] has been incorporated. The source terms for the k and ε equations are

$$S_k = G_k + G_B - \rho\varepsilon, \quad (6)$$

$$S_\varepsilon = C_1 \frac{\varepsilon}{k}(G_k + G_B)(1 + C_3 R_f) - C_2 \frac{\rho\varepsilon^2}{k}. \quad (7)$$

The generation terms are defined as follows:

(i) shear production

$$G_k = \mu_t \left(\frac{\partial u_i}{\partial x_j} + \frac{\partial u_j}{\partial x_i}\right)\frac{\partial u_i}{\partial x_j}, \quad (8)$$

(ii) buoyancy production

$$G_B = -\beta g_i \frac{\mu_t}{\sigma_t}\frac{\partial T}{\partial x_i}. \quad (9)$$

The flux Richardson number R_f appearing in equation (7) is defined as

$$R_f = -\frac{G_{\overline{v'^2}}}{2(G_k + G_B)} \quad (10)$$

where $G_{\overline{v'^2}}$ is the buoyancy production of the lateral energy component. In horizontal shear layers where the lateral velocity component is in the direction of gravity so that

$$G_{\overline{v'^2}} = 2G_B. \quad (11)$$

The above model contains seven constants, which are shown in Table 1.

3.3. *Mean stream curvature correction*

Body forces are known to have a strong effect on turbulence, and there is a close analogy between the effects of body forces due to buoyancy and those due to streamline curvature or rotation [12, 13]. In the present problem, the interaction between the buoyancy plume and forced ventilation flow contributes to the rates of diffusion of mass, momentum and heat. This situation is similar to those happening in the turbulent recirculating flows, such as the flow with a backward facing step. Therefore, the effect of the mean streamline curvature on turbulence should be taken into account.

Table 1. Constants in k–ε model

C_1	C_2	C_3	C_μ	σ_k	σ_ε	σ_t
1.44	1.92	0.8	0.09	1.0	1.3	1.0

It is known that [12], when the mixing length hypothesis is used for turbulent flow calculations, the effects of streamline curvature can be accounted for by empirically relating the mixing length to a suitable Richardson number that characterizes the relative importance of body force; the Monin–Oboukhov relation is a typical example. In the k–ε model, the k equation accounts directly for body forces because it is a direct consequence of the derivation from the Navier–Stokes equations. However, since the dissipation rate, ε ($\propto k^{3/2}/L$), is also determined from a transport equation, the question arises how body force effects should enter in such an equation. It is this question with which the present work is specially concerned.

There are many works concerning the effects of streamline curvature. Launder *et al.* [14] have suggested modifying the length scale equation for rotating flows by making constant C_2 in the ε-equation as a function of a gradient Richardson number. Lilley [15] has used a Richardson number in his correction of the length scale equation for swirling jets. To simulate a backward facing step flow over a two-dimensional fence, Durst and Rastogi [16] have modified the turbulence energy production to take account of the effects of the mean streamline curvature.

Stimulated by these studies, we propose to add the production due to streamline curvature to the body-force production G_B in the k and ε equations. It is noted that, besides the streamline curvature in the longitudinal direction (x–y plane), the significant secondary flow in cross-sections (y–z plane) should also be considered. Thus, G_B becomes

$$G_B = -\beta g \frac{\mu_t}{\sigma_t}\frac{\partial T}{\partial y} - \rho\overline{v_r' v_\theta'} r \frac{\partial v_\theta/r}{\partial r} - \rho\overline{v_s' v_\gamma'} s \frac{\partial v_\gamma/s}{\partial s}, \quad (12)$$

where

$$\rho\overline{v_r' v_\theta'} = -\mu_t r \frac{\partial v_\theta/r}{\partial r} \quad (13)$$

$$\rho\overline{v_s' v_\gamma'} = -\mu_t s \frac{\partial v_\gamma/s}{\partial s}. \quad (14)$$

In above equations, v_θ is the swirl velocity component and $\rho\overline{v_r' v_\theta'}$ is the tangential shear stress in x–y plane, v_γ is the swirl velocity component and $\rho\overline{v_s' v_\gamma'}$ is the tangential shear stress in y–z plane. Figure 3 should be referred to for the other nomenclature.

Consequently, the flux Richardson number is corrected to be

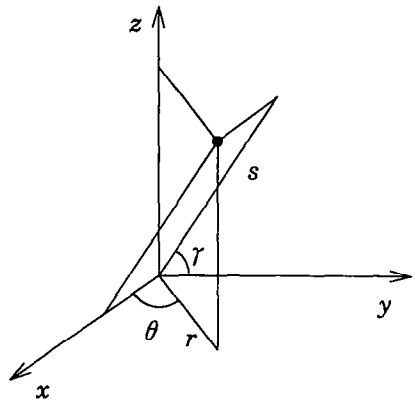

FIG. 3. Cylindrical coordinate system of r, θ, z and s, γ, x.

$$R_f = -\frac{G_B - 2\rho\overline{v_r'v_\theta'}v_\theta/r - 2\rho\overline{v_s'v_\gamma'}v_\gamma/s}{G_k + G_B}. \quad (15)$$

3.4. *Boundary and initial conditions*

There are three types of boundaries in the present problem, namely solid boundaries at the walls, free boundaries at the surface of the burner units and free boundaries at the inlet and the outlet. On solid walls, the no-slip condition for the velocity components is employed. The wall temperature, which is a time-dependent function of heat input to the tunnel, is given by the corresponding experimental measurements.

At the low-turbulence region close to the walls, the wall functions for velocity components and temperature are employed. Assuming the local equilibrium in this region, the kinetic energy of turbulence and the dissipation rate can be decided.

On the surface of the burner, the heat flux and normal velocity component are prescribed. At the inlet, all dependent variables are prescribed by the initial solution of a previous computation. At the outlet, for all dependent variables, zero-gradient conditions are prescribed.

The computation starts with the solution of a previous computation as an initial condition. At the previous computation, the tunnel is not heated and the ventilation air flow is taken as steady. The velocity distribution at the inlet is assumed uniform and the value of mean velocity is given by the experimental measurement. The values of k and ε at the inlet are empirically given as $k_{in} = 0.005u_0^2$ and $\varepsilon_{in} = C_\mu k^{3/2}/(0.03R)$, respectively. A uniform temperature distribution (set at the room temperature) is also assumed as an initial condition.

4. COMPUTATIONAL METHODS

Since the Cartesian system suffers severely from geometric limitations, the application of such a system to curved surfaces must involve interpolation between grid points not coincident with the boundaries. Otherwise, a huge grid number has to be employed. Besides, the Neumann type boundary condition is difficult to apply. In the present study, the geometric limitation is removed by adopting a general curvilinear coordinate system.

To simplify the calculation, the coordinate in x direction is retained to be Cartesian, only coordinates in y and z directions are transformed to general curvilinear system in order to fit the complicated cross-sectional geometry of a tunnel. A three-dimensional transformation relation is written here for generality.

4.1. *General curvilinear coordinate system*

As shown in Fig. 4, the transformation from the Cartesian coordinates (x, y, z) to curvilinear coordinates (ξ, η, ζ) is considered. Partial derivatives of any function f are transformed according to the chain rule

$$\begin{pmatrix} f_\xi \\ f_\eta \\ f_\zeta \end{pmatrix} = J \begin{pmatrix} f_x \\ f_y \\ f_z \end{pmatrix}, \quad (16)$$

where J represents Jacobian written as

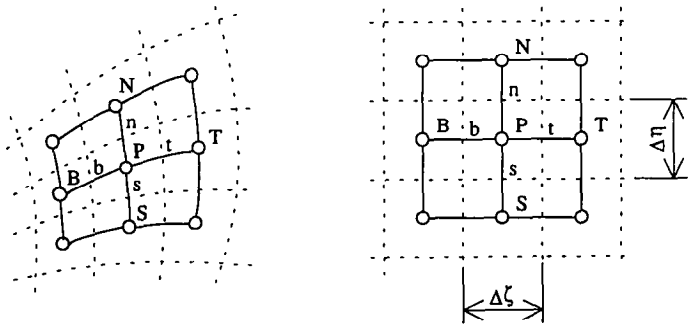

(a) Physical plane (b) Transformed plane

FIG. 4. Finite difference grid representation.

$$J=\begin{pmatrix} x_\xi & y_\xi & x_\xi \\ x_\eta & y_\eta & y_\eta \\ x_\zeta & z_\zeta & z_\zeta \end{pmatrix}. \tag{17}$$

The above equations can be used to transform the first-order differential terms into the curvilinear coordinates. But this will lead the governing equations to have many extra terms which are obviously not convenient for numerical calculation. Hence, the following inverse matrix of the chain rule is used,

$$\begin{pmatrix} f_x \\ f_y \\ f_z \end{pmatrix}=\begin{pmatrix} \xi_x & \eta_x & \zeta_x \\ \xi_y & \eta_y & \zeta_y \\ \xi_z & \eta_z & \zeta_z \end{pmatrix}\begin{pmatrix} f_\xi \\ f_\eta \\ f_\zeta \end{pmatrix}. \tag{18}$$

where ξ_x, η_y, ζ_z can be obtained by substituting ξ, η and ζ into f in equation (16).

4.2. *Numerical grid generation*

The grid generation scheme developed by Thompson *et al.* [17] is adopted. In this method, the curvilinear coordinates are generated by solving the Poisson equations

$$\nabla^2\zeta = P, \tag{19}$$

$$\nabla^2\eta = Q \tag{20}$$

in which the 'control functions' P and Q can be fashioned to control the spacing and orientation of the coordinate lines [17].

The generated grid for the tunnel cross-section is shown in Fig. 5. The present computations are performed on $36\times 13\times 11$ grids.

4.3. *Transformation of the governing equations*

The set of conservation equations can be written in the following general form:

$$\frac{\partial\rho}{\partial t}+\frac{\partial(\rho u_i)}{\partial x_i}=0, \tag{21}$$

$$\frac{\partial(\rho\Phi)}{\partial t}+\frac{\partial(\rho u_i\Phi)}{\partial x_i}=\frac{\partial}{\partial x_i}\left(\Gamma\frac{\partial\Phi}{\partial x_i}\right)+S_\Phi. \tag{22}$$

The contravariant velocity components are defined as

$$U=(\xi_x u+\xi_y v+\xi_z w)J, \tag{23}$$

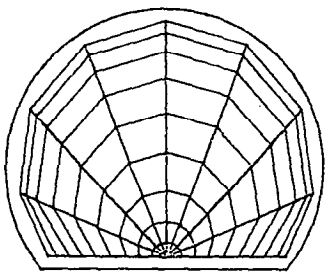

FIG. 5. Grid detail of cross-section.

$$V=(\eta_x u+\eta_y v+\eta_z w)J, \tag{24}$$

$$W=(\zeta_x u+\zeta_y v+\zeta_z w)J. \tag{25}$$

With equations (23)–(25), the set of conservation equations can be transformed into ξ–η–ζ curvilinear coordinates as

$$\frac{J\partial\rho}{\partial t}+\frac{\partial(\rho U)}{\partial\xi}+\frac{\partial(\rho V)}{\partial\eta}+\frac{\partial(\rho W)}{\partial\zeta}=0, \tag{26}$$

$$\begin{aligned}\frac{J\partial(\rho\Phi)}{\partial t}&+\frac{\partial(\rho U\Phi)}{\partial\xi}+\frac{\partial(\rho V\Phi)}{\partial\eta}+\frac{\partial(\rho W\Phi)}{\partial\zeta}\\ &=\frac{\partial}{\partial\xi}[\Gamma J(q_{11}\Phi_\xi+q_{12}\Phi_\eta+q_{13}\Phi_\zeta)]\\ &\quad+\frac{\partial}{\partial\eta}[\Gamma J(q_{21}\Phi_\xi+q_{22}\Phi_\eta+q_{23}\Phi_\zeta)]\\ &\quad+\frac{\partial}{\partial\zeta}[\Gamma J(q_{31}\Phi_\xi+q_{32}\Phi_\zeta+q_{33}\Phi_\zeta)]+JS_\Phi\end{aligned} \tag{27}$$

where q_{ij} is the metric of transformation.

4.4. *Pressure-correction equation*

In terms of the notation shown in Fig. 4, a relation between Φ at the point P and the neighboring values can be written in the following discretization equation:

$$a_P\Phi_P=\sum_{nb}a_{nb}\Phi_{nb}+b \tag{28}$$

where nb represents neighbor grid point and the coefficients are modified according to a hybrid scheme.

In a finite-difference method, if the velocity components and pressure are located at the same grid points, a checkerboard pressure field can develop as an acceptable solution. This is described fully in Patankar [18]. Although the staggered grid eliminates major difficulties, it introduces inconvenience, which becomes more serious when the method is extended to curvilinear nonorthogonal coordinates. On the consideration of computational speed and accuracy, Peric *et al.* [19] strongly recommended the use of the collocated grid when a three-dimensional geometry and general curvilinear coordinates are considered.

Rhie and Chow [20] presented a method that employs a nonstaggered grid in curvilinear nonorthogonal coordinates. Similar to their method, the velocity components and all the other variables are located at the common grid positions. The velocity and pressure are coupled by a simple but effective scheme to suppress the pressure oscillations.

Following the control-volume formulation, the discretization of the momentum equation in ξ direction can be written as

$$u_P=\frac{\Sigma a_{nb}u_{nb}+b_u}{a_P}-\frac{J}{a_P}\Delta\eta\,\Delta\zeta[(\xi_x p)_e-(\xi_x p)_w]$$

Table 2. Experimental and calculation conditions

Case	u_0 (m s^{-1})	Re_D	q (W m^{-2})	S_h† (m^2)	Gr^*	u_h (m s^{-1})	T_0 (°C)
1	0.46	11 332	1.42×10^5	0.0216	2.30×10^{13}	0.104	19.5
2	0.92	22 808	1.42×10^5	0.0216	2.28×10^{13}	0.084	18.5

† Two central burner units were used.

$$-\frac{J}{a_P}\Delta\xi\,\Delta\zeta[(\eta_x p)_n-(\eta_x p)_s]$$

$$-\frac{J}{a_P}\Delta\xi\,\Delta\eta[(\zeta_x p)_t-(\zeta_x p)_b]. \quad (29)$$

With the linear interpolation between grid nodes E and P, the velocity components u_c can be obtained, while the interpolated pressure gradient term based on the $2\Delta\xi$-center difference is replaced by the $1\Delta\xi$-center difference on the cell boundary,

$$u_c=\frac{\overline{\Sigma a_{nb}u_{nb}+b_u}}{a_P}-\frac{\bar{J}}{a_P}\Delta\eta\,\Delta\zeta[(\xi_x p)_E-(\xi_x p)_P]$$

$$-\overline{\frac{J}{a_P}\Delta\xi\,\Delta\zeta[(\eta_x p)_n-(\eta_x p)_s]}$$

$$-\overline{\frac{J}{a_P}\Delta\xi\,\Delta\eta[(\zeta_x p)_t-(\zeta_x p)_b]} \quad (30)$$

where over-bar represents the interpolated value between grid nodes E and P. This procedure ensures strong velocity–pressure coupling. The similar treatment is also applied to the momentum equations in η and ζ directions.

4.5. *Solution procedure*

The SIMPLER algorithm [18] is extended to a general curvilinear coordinate system with collocated grids. To decide whether a solution is converged, the overall mass balance is used. Convergence is declared when maximum line errors have dropped below 0.5%. The calculations were carried out on the Hitachi M-880 computer at the Computer Center of the University of Tokyo. It takes about 7 s of CPU time to calculate one time step.

5. RESULTS AND DISCUSSION

The results of the computations were compared with the experimental data. The comparisons were made between the computational and experimental transient temperature profiles in the cross-sections of the tunnel. The ability of the model to predict the location of the leading edge of the heated air flow was also validated. Two experimental and calculation conditions are listed in Table 2.

The predictions were compared with measurements at six heights on the center line of the tunnel. Figure 6 shows the comparison of the transient temperature profiles for Case 1, where (a) is for a cross-section relatively near the burner whereas (b) is for a cross-section relatively far downstream. Symbols represent measured values whereas lines represent the calculated results. The discrepancies between the prediction and the measurement are large in (a), but in (b) reasonable agreement is achieved.

Figure 7 compares the transient temperature profiles for Case 2. Discrepancies still remain considerable where the cross-section is close to the burner. But for the cross-section downstream, good agreement between measured and predicted temperatures is obtained.

There are two causes which may be considered for the unsatisfactory predictions of temperature distribution at the cross-sections close to the burner. One is that the behavior of the heated air flow near the burner is largely affected by the combustion which is not included in the present model. The other is that the burner unit contains a number of small nozzles. To simulate the detail behavior of the blowing of air–gas mixture, it is necessary to place at least one grid

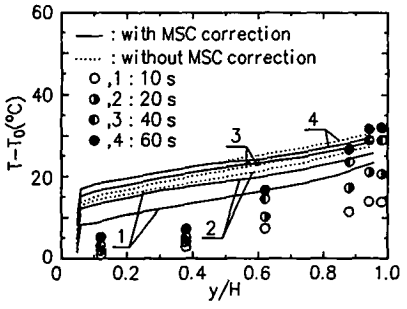

(a) x/H=2.46

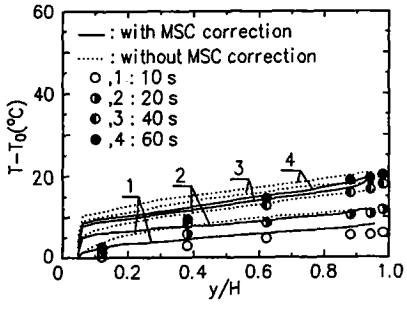

(b) x/H=9.85

FIG. 6. Predicted and measured temperature profiles (Case 1).

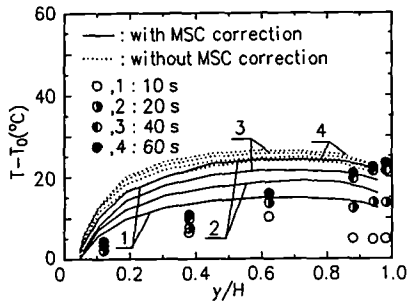

(a) x/H=2.46

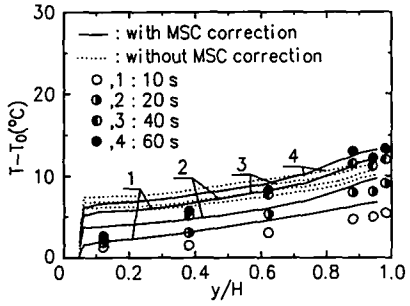

(b) x/H=9.85

FIG. 7. Predicted and measured temperature profiles (Case 2).

at each nozzle and four at its boundaries. This will lead to a huge grid number in the present calculation. As a result of compromise on computational cost, the mean blowing velocity v_h is used for the boundary condition. The burner unit is simplified as a uniform heat and mass output source. The simplification is considered to affect the simulated behavior of the heated air flow near the burner.

Velocity vectors and isotherms on the plane of symmetry and some cross-section can be seen in Figs. 8 and 9 for Case 2 after 40 s of heating of the tunnel. Owing to the effect of forced ventilation, the reverse flow is not formed in Fig. 8. Some streamline curvature can be observed close to the burner. In Fig. 9, strong secondary flows are observed. The velocity components on the cross-sections close to the burner are several times larger than the ones on downstream cross-sections. There are two kinds of secondary flow patterns appearing in Fig. 9. At $x/H = 2.46$, only two large swirls are symmetrically formed in the center of the cross-section, but at $x/H = 9.85$ and the other two downstream cross-sections, two small swirls appear at both left and right floor corner.

The streamline curvature formed in the region close to the burner did give a large influence on turbulence. When the numerical model without correction of mean streamline curvature is applied to the situations shown in Figs. 6 and 7, it is found that the discrepancies between the measurements and predictions are large. The finding is not surprising because other workers who have calculated boundary layer flow over curved surface or recirculating flow [15, 16] without introducing the correction on the effects of the streamline curvature have likewise found poor agreement. For further validations, the correction of streamline curvature is also applied to our previous study [8]. The two-dimensional test section used in the study is 2.95 m long with a uniform cross-section 0.5 m wide by 0.1 m high. The heat source is simulated by an electrical heater which is made of spiral Nichrome wire.

The results presented in Fig.10 compare the transient temperature profiles at two cross-sections with and without mean streamline curvature correction, when $q = 2.92 \times 10^4$ W m^{-2} and $u_0 = 0.37$ m s^{-1}. The good agreement between the prediction and the measurement is achieved.

The work of Launder and Morse [21] on swirling jets indicated that the coefficient C_μ in the k–ε model is increased by the effect of swirl. When such an increase is allowed for, a smaller value of C_3 is needed to achieve the agreement with measurements. Durst and Rastogi [18] studied a turbulent recirculating flow

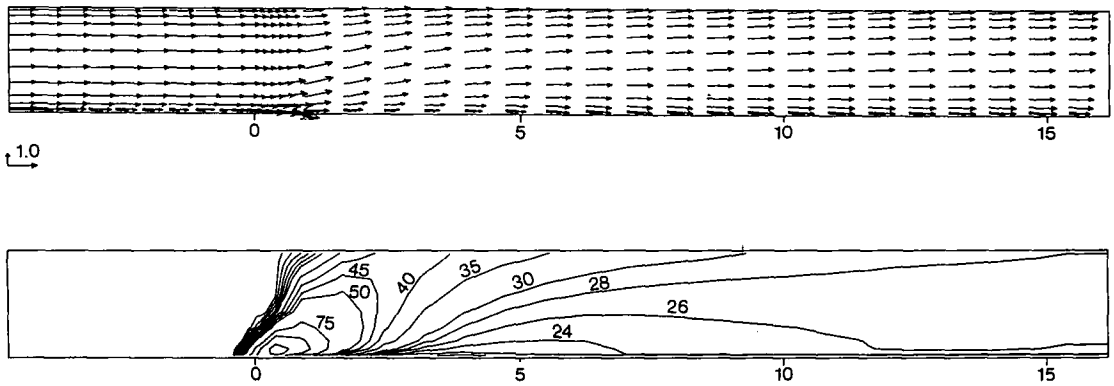

FIG. 8. Calculated velocity vectors and isotherms (Case 2) (x–y plane, $y/H = 0$, $t = 40$ s, unit: °C).

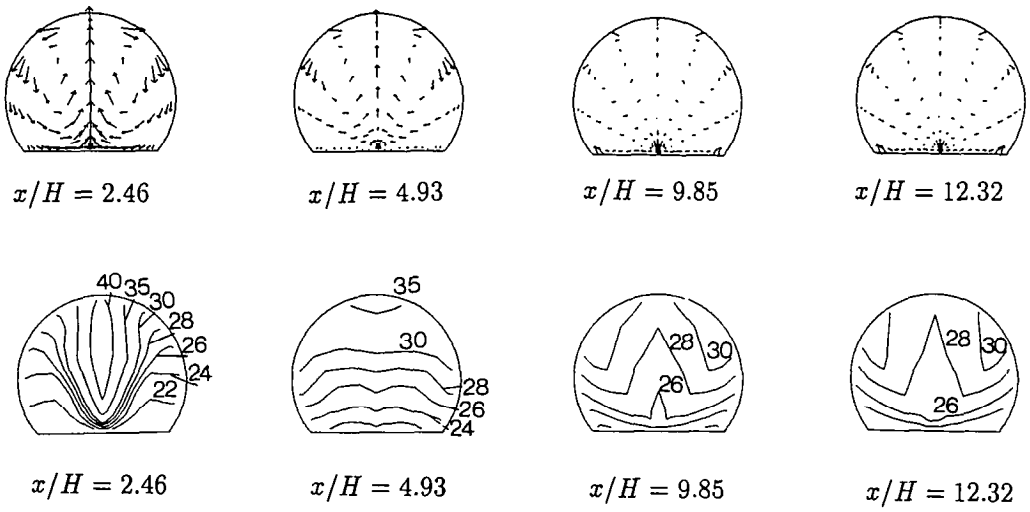

FIG. 9. Calculated velocity vectors and isotherms (Case 2) (z–y plane, t = 40 s, unit: °C).

and modified the length scale equation by making a mean streamline correction on the constant C_2. The present correction qualitatively agrees with their suggestions. The body force production G_B in the ε equation should be multiplied by a coefficient much smaller than that for shear production G_k, when the vertical shear becomes stronger. The corrections are directly applied to the production term, because the body force term enters the length scale equation.

An immediate consequence of the heated air flowing near the ceiling is the spreading of the combustion plume along the ventilation. The leading edge of the heated air flow in x direction, which is defined as a position where the fluid temperature is increased by 1°C, has been measured and calculated.

The measurements of the leading edge of the heated air flow are made by 15 thermocouples in the symmetrical plane along x direction. The thermocouples are installed at a height $y/H = 0.62$. The results are shown in Fig. 11. The variable x_F/H is considered as an important parameter for fire hazard evaluation. As is seen from the result, we are able to predict the leading edge of the heated air flow with the present numerical model.

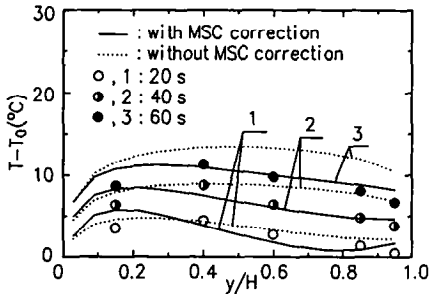

(a) x/H=2.1

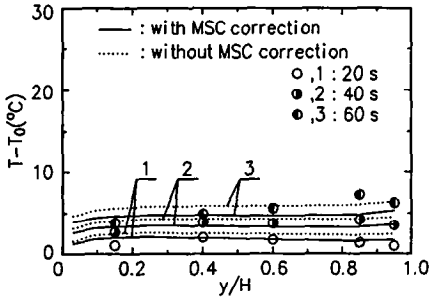

(b) x/H=12.6

FIG. 10. Predicted and measured temperature profiles (two-dimensional case, $q = 2.92 \times 10^4$ W m^{-2}, $u_0 = 0.37$ m s^{-1}).

5. CONCLUSIONS

The mathematical model described and applied here represents the application of the developing subject of computational fluid dynamics to fires in ventilated road or railway tunnels. The model attempts

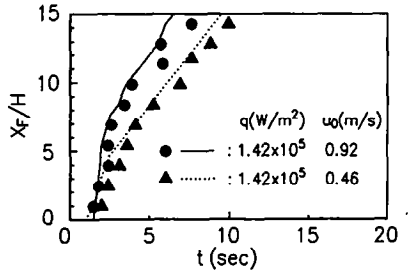

FIG. 11. Leading edge of the heated air flow.

to retain as much of the rigor and generality of the governing equations of conservation of mass, momentum, and energy as possible. It makes no assumptions about how the fire behaves other than the heat release rate and a vertical velocity component in the transient calculation. The computational code adopting a general curvilinear coordinate system can be applied to any geometric shape of tunnels.

The predictions have been compared with the experimental data and shown to be in reasonable agreement except in the region close to the burner. The present model can be used to predict the leading edge of the heated air flow which is directly relevant to the safety considerations in tunnel fires. Although the model has been tested in a few cases for validation purposes, little difficulty would be expected from the incorporation of effects such as external wind pressures or traffic-induced air movement.

It has been recognized that the standard k–ε model does not allow precise representation of the present problem. Some improvements have been provided in the present numerical models on accounting for the influence of buoyancy and mean streamline curvature on turbulence.

For simulating the influence of mean streamline curvature on turbulence, some advanced turbulence models (e.g. ref. [22]) have been developed. The emphasis of the present work is to apply it in the framework of k–ε turbulence model. Because of its significant physical basis and universality, the present model is also recommended for the modeling of other related engineering practices.

Real fires appear to have significant density variations which further complicate the turbulent flow. The conventional averaged field equations may, therefore, not be the best choice and other models, for example, the method of Favre-averaging, where density is not treated as a dependent variable, might be an alternative. On the other hand, species concentration transport also influences buoyancy and should be incorporated, particularly in reacting (or combustible) flows. Development of such a model and computational code will be the subject of future work.

Acknowledgements—The authors are grateful to Prof. H. Ohashi, Prof. M. Hirata, Prof. S. Kotake, Prof. I. Tanasawa, Dr T. Yamanaka, Mr Y. Kitahara and Mr Y. Watanabe for their helpful comments.

REFERENCES

1. J. Quintiere, B. J. Macaffery and T. Kashiwagi, A scaling study of a corridor subject to a room fire, *Combust. Sci. Technol.* **18,** 1–19 (1978).
2. R. Emori and K. Saito, Model rules on motion of smoke and gases in building fires, *Bull. Jap. Ass. Fire Sci. Engng* **29**(2), 41–49 (1979) (in Japanese).
3. J. De Ris, Duct fires, *Combust. Sci. Technol.* **2,** 239–258 (1970).
4. C. C. Hwang, R. F. Chaiken, J. M. Singer and D. H. N. Chi, Reverse stratified flow in duct fires: a two-dimensional approach, *16th Symposium (International) on Combustion*, pp. 1385–1395. MIT, Cambridge, MA (1977).
5. C. C. Hwang and J. D. Wargo, Experimental study of thermally generated reverse stratified layer in a fire tunnel, *Combust. Flame* **66,** 171–180 (1986).
6. J. Brandeis and D. J. Bergmann, A numerical study of tunnel fires, *Combust. Sci. Technol.* **35,** 133–155 (1983).
7. S. Koto and G. Yamanaka, Air flow analyses in a longitudinally ventilated road tunnel on fire, *Trans. Japan Soc. Mech. Engrs* **53**(494), 2937–2943 (1987) (in Japanese).
8. H. Xue, E. Hihara and T. Saito, Modeling of air flow in a fire tunnel, *Trans. Japan Soc. Mech. Engrs* **57**(536), 1457–1462 (1991) (in Japanese).
9. A. G. Gaydon and H. G. Wolfhard, *Flames, Their Structure, Radiation and Temperature*. Chapman and Hall, London (1970).
10. D. B. Spalding, *Turbulence models*, Report HTS/76/17, Imperial College Mechanical Engineering Dept., London (1976).
11. W. Rodi, *Turbulence Models and Their Application in Hydraulics—A State of the Art Review*. Book Publication of International Association for Hydraulic Research, Delft, Netherlands (1980).
12. P. Bradshaw, The analogy between streamline curvature and buoyancy in turbulent shear flow, *J. Fluid Mech.* **36,** 177–191 (1969).
13. P. Bradshaw, Effects of streamline curvature on turbulent flow, *AGARDograph*, No. 169 (1973).
14. B. E. Launder, C. H. Priddin and B. I. Sharma, The calculation of turbulent boundary layers on spinning and curved surfaces, *ASME J. Fluid Engng* **99,** 231–239 (1977).
15. D. G. Lilley, Prediction of inert turbulent swirl flows, *AIAA J.* **11**(7), 955–960 (1973).
16. F. Durst and A. K. Rastogi, Turbulent flow over two-dimensional fences, *Proc. 2nd Symposium on Turbulent Shear Flows*, pp. 218–232. Springer, London (1979).
17. J. F. Thompson, Z. U. A. Warsi and C. Wayne Mastin, *Numerical Grid Generation*. North-Holland, New York (1985).
18. S. V. Patankar, *Numerical Heat Transfer and Fluid Flow*. McGraw-Hill, New York (1980).
19. M. Peric, R. Kessler and G. Scheuerer, Comparison of finite-volume numerical method with staggered and collocated grids, *Computers Fluids* **16,** 316–324 (1988).
20. J. G. Rhie and W. L. Chow, A numerical study of the turbulent flow past an isolated airfoil with trailing edge separation, *AIAA J.* **21,** 1525–1532 (1983).
21. B. E. Launder and A. Morse, Numerical prediction of axisymmetric free shear flows with a second-order Reynolds stress closure. In *Proc. Turbulent Shear Flow 1*, pp. 279–294. Springer, Heidelberg (1979).
22. B. Gebhardt, Buoyancy induced fluid motions characteristic of applications in technology, *ASME J. Fluid Engng* **101,** 5–28 (1979).